Resonance avoidance for variable speed rotor blades using an applied compressive load

Robert Dibble*, Vaclav Ondra, Branislav Titurus

Department of Aerospace Engineering, University of Bristol, Bristol, BS8 1TH, UK

Abstract

Varying the rotational speed of the main rotor is one method being considered to improve the performance of future rotorcraft. However, changes in rotor speeds often lead to resonant interactions between rotor blade modes and the rotor's excitation frequencies which increase the vibratory loads in the rotor. This research investigates the use of a compressive load to reduce a blade's natural frequencies and its potential to be used as a resonance avoidance technique by improving separation between the natural and excitation frequencies of a blade. The research presented herein describes and validates a model of a pretwisted rotating beam with non-coincident mass and elastic axes with an applied compressive load. The compressive load is applied at the elastic axis at the tip of the beam and is orientated towards the root of the beam. The beam model is then used in a case study to represent the rotor blade of a typical mid-sized civilian helicopter. The case study is performed to calculate the natural frequencies of a compressed blade for a reduction in rotor speed of up to 40% and evaluate the performance of the compressive load resonance avoidance technique. The results of the case study show that the compressive load improves the separation between natural and excitation frequencies over the full range of rotor speeds evaluated. The improved separation allows the rotor to operate safely with a reduction in rotor speed of up to 19%.

Keywords

Boundary value problem; Blade dynamics; Variable speed rotor; Compressively loaded beams; Modal tuning; Resonance avoidance

1 Introduction

The rotary wing sector strives towards developing aircraft with increased performance capability and reduced emissions. One concept to achieve this is variable speed rotors which have been shown to require less power [1, 2, 3], expand flight envelopes [4, 5], reduce noise emissions [4, 6] and reduce fatigue , thereby reducing operating costs and allowing for relaxed maintenance schedules [7]. This concept is utilised in the Boeing A160T Hummingbird [8] which holds the endurance flight record for new and experimental technologies at over eighteen hours [9]; partly due to its ability to reduce its rotor speed by up to 40% [10]. The variable rotor speed concept is also utilised by tiltrotors which change their rotor configuration between helicopter mode and airplane mode. For instance, the V22 Osprey exhibits a reduction of 18% from the nominal rotor speed [11].

* Corresponding author. E-mail address: robert.dibble@bristol.ac.uk

Whilst variable speed rotors can achieve significant performance improvements, they encounter substantial dynamics complications [4, 12]. A rotor operating with insufficient separation between natural and excitation frequencies of the blade will incur resonance which leads to increased vibratory loads that negatively affect the blade's structural performance. Both the natural and excitation frequencies depend on rotor speed. Therefore, achieving sufficient separation over a wide range of rotor speeds is difficult using the design of the blade alone.

Therefore, rotorcraft are traditionally designed to operate at a fixed rotor speed with sufficient separation between all natural and excitation frequencies. If the benefits of variable speed rotors are to be fully utilised, a method to avoid these resonances or minimise their consequences must be developed.

Existing active methods for vibration control, such as Individual Blade Control [13, 14], may potentially be adapted to overcome the dynamics problems associated with variable speed rotors. However, active methods are often complex, heavy and have significant power requirements; typically, about 1% of vehicle weight and 3% of installed power [15]. Active methods also have the potential to exacerbate vibration problems during power failure [16]. Embedded dampers [10] are one passive method that have been explored to control loads in variable speed rotors. Whilst good results have been shown, this method is traditionally used to target a single predefined frequency. Alternatively, resonance avoidance can be achieved in variable speed rotors by designing stiff blades with natural frequencies that are high enough to avoid interactions with the excitation frequencies with the highest energy. However, this increase in stiffness can lead to a 34% increase in blade mass when compared to a conventional blade [1].

The potential of a compressive load to reduce a blade's natural frequencies and be used as a resonance avoidance technique is studied in this paper. The use of compressive loading to control the dynamic properties of helicopter tail booms has previously been studied [17]. However, the use of compressive loading to alter the dynamic properties of a rotor blade is a novel area of research. In previous work [18, 19], it has been demonstrated that reductions in natural frequencies of up to 10% of the rotor frequency can be achieved for the simplified case of uncoupled motions. In this study, the compressive load is modelled as a force as this allows the effects of the force to be isolated from any secondary effects of the load application system [18, 20]. The load application system and any associated effects of it are considered a separate area of research. The research presented herein aims to validate the modelling technique for a pretwisted rotating beam with non-coincident mass and elastic axes and to demonstrate the potential of compressive loading as a resonance avoidance technique for variable speed rotors.

The paper is organised as follows: in section 2 a beam model with coupled motions and an applied compressive load is presented; in section 3 the frequency calculations of this model are verified and validated against those from a bench-top experiment and a Finite Element (FE) model; finally, in section 4 the developed model is used in a case study to demonstrate the ability of compressive loading to increase the separation between natural and excitation frequencies for a mid-sized civilian rotorcraft with a variable speed rotor.

2 Mathematical model of a rotating beam subjected to compressive load

To investigate the influence of compressive loading on a rotor blade's dynamic properties a suitable low order model is developed. Due to the prismatic nature and high aspect ratio of rotor blades, typical values between 10 and 20 [21], it is common to model them as beams. Whilst the method for applying the compressive load is not considered explicitly, it is expected that it will consist of a tendon attached to the tip of the blade and actuated from the blade's root. Therefore, the force used in the model will be situated at the tip of the deformed blade and orientated towards its root as visualised in Fig. 1; where x, y, z represent the orthogonal coordinate system defined such that the x axis rotates with the beam and lies along the initial undeformed position of the elastic axis and the z axis is the axis of rotation, R is the radius of the beam, R_0 is the radial location of the beam's root, and Ω is the angular velocity of rotation.

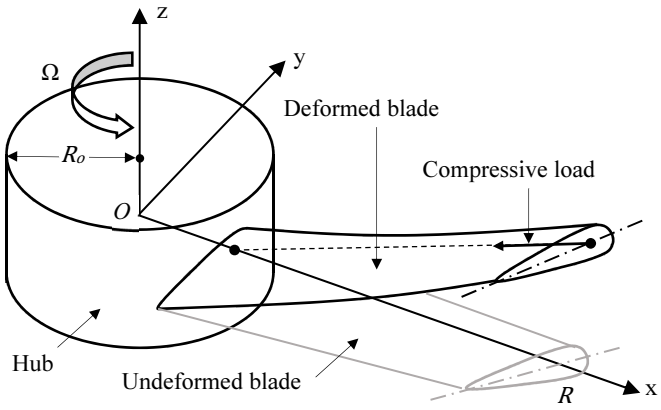

Fig. 1. Compressive loading concept

The equations of motion derived by Houbolt and Brooks [22] represent rotating pretwisted beams with non-coincident mass and elastic axes that exhibit coupling between their torsional motion and their translational motion in- and out-of- the plane of rotation. Due to their ability to capture such phenomena they are ideally suited for modelling rotor blades, as shown by their adoption in industry developed blade analysis codes, J134 [23] and S4 [24]. Therefore, the subsequent mathematical model shall be based upon these equations.

2.1 Boundary value problem

The model is formulated as an eigenvalue Boundary Value Problem (BVP) and solved numerically using a collocation method [25]. The results are used to provide the modal properties of a rotating beam over a range of predefined rotor speeds and compressive loads.

2.1.1 Field equations

The aforementioned equations of Houbolt and Brooks [22] are a set of three, linear, non-homogenous, partial differential equations defined on one spatial domain and one temporal domain. These equations are based on Euler-Bernoulli theory, which

neglects the sectional transverse shear deformation, rotary inertia effects and warping [26]. It is assumed that the motion of the beam is harmonic (normal mode assumption) which allows the principle of separation of variables to be employed, such that the temporal domain is removed. The resulting equations are a set of Ordinary Differential Equations (ODEs) that are used to evaluate the modal properties of the beam

$$\begin{aligned}&[(EI_2 - EI_1)\sin\beta\cos\beta\, w'' + (EI_1(\sin\beta)^2 + EI_2(\cos\beta)^2)v'' + Te_A\phi\sin\beta]'' - (Tv')' + (\Omega^2 mxe\phi\sin\beta)' \\ &\quad + \Omega^2 me\phi\sin\beta - m\omega^2(v - e\phi\sin\beta) - \Omega^2 mv = 0\end{aligned}$$

$$\begin{aligned}&[(EI_1(\cos\beta)^2 + EI_2(\sin\beta)^2)w'' + (EI_2 - EI_1)\sin\beta\cos\beta\, v'' - Te_A\phi\cos\beta]'' - (Tw')' - (\Omega^2 mxe\cos\beta\,\phi)' \\ &\quad - m\omega^2(w + e\phi\cos\beta) = 0\end{aligned} \tag{1}$$

$$\begin{aligned}&-\left\{\left[GJ + Tk_A{}^2\right]\phi'\right\}' + Te_A(v''\sin\beta - w''\cos\beta) + \Omega^2 mxe(-v'\sin\beta + w'\cos\beta) \\ &\quad + \Omega^2 m\left[\left(k_{m2}{}^2 - k_{m1}{}^2\right)\cos 2\beta + ee_0\cos\beta\right]\phi + \Omega^2 me\sin\beta\, v - \omega^2 mk_m{}^2\phi \\ &\quad - me\omega^2(-v\sin\beta + w\cos\beta) = 0\end{aligned}$$

where $v(x)$ and $w(x)$ are the transversal deformations in- and out-of- the plane of rotation, respectively, $\phi(x)$ is the angle of twist deformation, e is the distance between the mass and the elastic axis, e_A is the distance between the area centroid of the tensile member and the elastic axis, e_0 is the fore-aft distance at the root between the elastic axis and the z axis about which the beam is rotating, J is the torsional stiffness constant, k_A is the polar radius of gyration of the cross-sectional area, k_m is the polar radius of gyration of the cross-sectional mass about the elastic axis, k_{m1} and k_{m2} are the mass radii of gyration about the major neutral axis and about a perpendicular axis through the elastic axis respectively, $T(x)$ is the tension, $\beta(x)$ is the beam pretwist prior to any deformation, [ ]' is the derivative with respect to x.

2.1.2 Compressive load model

In this study the applied compressive load is modelled as a force at the elastic axis of the tip of the beam directed towards its root. This load is decomposed into forces acting along the undeformed x, y and z axes, similarly to [27], as seen in Fig. 2 where P is the applied compressive load and P_x, P_y and P_z are the compressive load components in the x, y, z directions respectively as defined below using the geometry of the deformed beam.

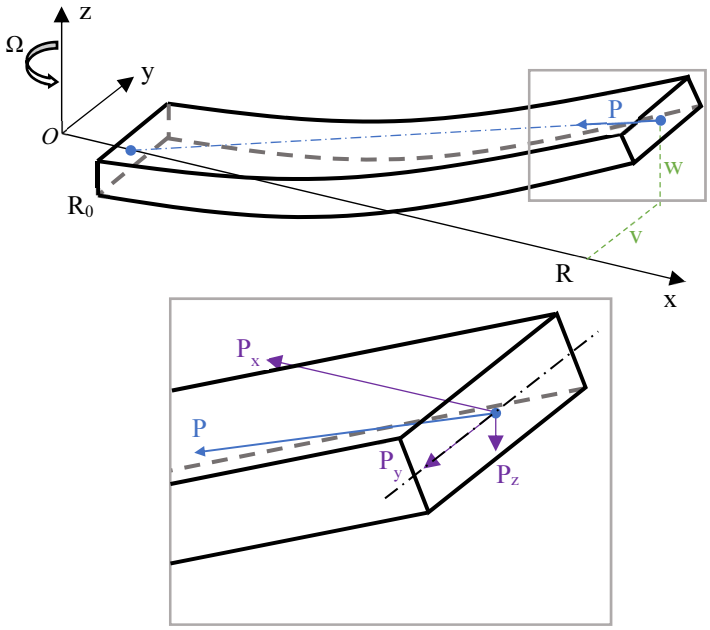

Fig. 2. Schematic of compressive force decomposition

The components of the compressive load are defined using the geometry of the beam and its deformation as seen in Eq (2).

$$P_x = P\frac{R - R_0}{\sqrt{(R - R_0)^2 + v(R)^2 + w(R)^2}}$$

$$P_y = P\frac{v(R)}{\sqrt{(R - R_0)^2 + v(R)^2 + w(R)^2}}v \tag{2}$$

$$P_z = P\frac{w(R)}{\sqrt{(R - R_0)^2 + v(R)^2 + w(R)^2}}w$$

It is assumed that $R - R_0 \gg v(R)$ and that $R - R_0 \gg w(R)$ such that $\sqrt{(R - R_0)^2 + v(R)^2 + w(R)^2} \approx R - R_0$, which linearises the force components with respect to v and w.

$$P_x \approx P$$

$$P_y \approx \frac{P}{R - R_0}v(R) \tag{3}$$

$$P_z \approx \frac{P}{R - R_0}w(R)$$

The internal tension in the beam is governed by two separate effects. The first effect pertains to the centrifugal force and is governed by the mass of the beam and its rotational speed. The second effect is the reduction in tension due to the component of the compressive load acting along the x axis. The internal tension, defined below, is present in the field equations, Eq. (1), and the boundary conditions in section 2.1.3.

$$T = \int_x^R \Omega^2 m\hat{x}\, d\hat{x} - P_x \approx \frac{1}{2}\Omega^2 m(R^2 - x^2) - P \tag{4}$$

For this research, the force is directed towards the root as this is a possible point of attachment of a system used to apply the compressive loading. However, an additional benefit of this modelling methodology is that it could be generalised, by modifying Eq. (3), for an arbitrary tendon orientation which would benefit future investigations into alternative attachment locations, such as the pitch horn or rotor hub.

2.1.3 Boundary conditions

Cantilevered boundary conditions are enforced to represent a bearingless hub as can be found in modern helicopters. The boundary conditions at the root of the beam, $x = R_0$, consist of constraining displacements and slopes to zero as defined in Eq. (5).

$$\begin{gathered} v = 0 \\ w = 0 \\ \phi = 0 \\ v' = 0 \\ w' = 0 \end{gathered} \tag{5}$$

The conditions enforced at the tip of the beam, $x = R$, ensure force and moment equilibriums between the internal beam loads and any applied loads. Traditional cantilevered boundary conditions have no applied loads at the tip and can be expressed as in Eq. (6) [22]

$$\begin{gathered} Q = 0 \\ M_y = 0 \\ M_z = 0 \\ F_y = 0 \\ F_z = 0 \end{gathered} \tag{6}$$

where Q is the internal torque about the elastic axis, M_y and M_z are the internal moments about the y and z axes, F_y and F_z are internal shear forces in the y, z directions. These terms are defined as follows

$$Q = \left[GJ + Tk_A{}^2\right]\phi'$$

$$M_y = (EI_1(\cos\beta)^2 + EI_2(\sin\beta)^2)w'' + (EI_2 - EI_1)\sin\beta\cos\beta\, v'' - Te_A\phi\cos\beta$$

$$M_z = (EI_1(\sin\beta)^2 + EI_2(\cos\beta)^2)v'' + (EI_2 - EI_1)\sin\beta\cos\beta\, w'' + Te_A\phi\sin\beta \quad (7)$$

$$F_y = Tv' - M_z' - \Omega^2 mex\sin(\beta)\,\phi$$

$$F_z = Tw' - M_y' + \Omega^2 mex\cos(\beta)\,\phi$$

These boundary conditions are modified here to include the effects of the compressive load. The influence of the component of the compressive load in the x direction is present in Eq. (7) via the terms containing T, as can be seen from Eq. (4). The components of the compressive load in the y and z directions are included as applied forces in the boundary conditions. Due to the definition of these forces seen in Fig. 2, a negative sign is introduced to ensure both the internal and applied loads are positive when acting in the y, z directions. The inclusion of these forces results in the following boundary conditions.

$$Q = 0$$

$$M_y = 0$$

$$M_z = 0 \quad (8)$$

$$F_y = -P_y$$

$$F_z = -P_z$$

A final boundary condition at the tip of the beam is introduced to normalise the eigenvectors. This condition is formulated such that it captures the magnitude of the deformation in each direction. This necessitates a scaling term for the torsion deformation to compare it with the in-plane and out-of-plane translations.

$$v^2 + w^2 + (\alpha\phi)^2 = 1 \quad (9)$$

where α is a scaling term chosen based on a characteristic cross-section dimension.

2.2 BVP solution approach

Collocation is used to numerically solve the BVP, described in 2.1. The collocation solver used is *bvp4c*, a native solver within *MatLab* [28]. In addition to the BVP, an initial estimate for the solution is required. This initial estimate must be sufficiently similar to the final solution to ensure that the solver converges to the desired solution.

To calculate a suitable initial estimate for the eigenvalue analysis, an associated harmonic BVP is formulated. This BVP omits the modeshape normalisation condition, Eq. (9), and introduces additional harmonic forcing. The forcing is formulated as a set of three orthogonal moments of magnitude M_{excite}, oscillating at a frequency, ω, in the in-plane, out-of-plane and torsional directions at the tip of the beam. These forcing moments are implemented as additional moments in the moment and torque boundary conditions defined in Eq. (8). The solutions of this BVP are the forced responses which are used to identify potential modes within the frequency domain and provide initial estimates for the eigenvalue analyses.

2.3 Parametric analysis procedure

A two-part procedure is used to calculate the modal properties of the beam over a range of rotor speeds and compressive loads. In part one, the desired number of modes are calculated for a single value of rotor speed and compressive load. Once the desired modes have been obtained, part two recalculates these modes for each combination of rotor speed and compressive load.

The first part of this procedure, to calculate the modes at a single rotor speed and compressive load, uses a combination of harmonic and eigenvalue analyses. A frequency sweep using harmonic analyses is performed. The sweep is initialised at a low frequency using an analytical solution for an uncoupled beam [29] as the initial estimate for the solver. The frequency is then incrementally increased and the solution from the previous iteration is used as the initial estimate for the current iteration. The size of the frequency step, $\Delta\omega$, is chosen to ensure a numerically stable solution procedure.

The solutions of these harmonic analyses are used to identify the presence of a mode using two separate identification conditions. One condition identifies resonance using the response of the tip of the beam and the other condition evaluates the orthogonality of the response shape against a known modeshape [30]. The combination of these two conditions ensures a robust identification of all modes.

Once a mode is detected by either of these conditions, the closest corresponding harmonic response is used as the initial estimate to initialise an eigenvalue analysis that calculates the natural frequency and mode shape. This process is repeated until the desired number of modes have been calculated and is shown in Fig. 3.

```
Omega = initial rotor speed
P = initial compressive load
ω = ~0
initial shape = analytical solution
while not all modes found
    forced response = harmonic analysis (initial shape)
    if response indicates mode
        eigenvalue = eigenvalue analysis (forced response)
    end
    ω = ω + Δω
    initial shape = forced response
end
```

Fig. 3. Process of natural frequency and mode shape calculation for initial rotor speed and compressive load.

Once the natural frequencies are calculated for a single value of rotor speed and compressive load in part one, the natural frequencies for all the combinations of the predefined rotor speed and compressive loading ranges are calculated. Firstly, a sweep of rotor speeds is performed while the compressive load remains constant. The rotor speed is incrementally increased, and eigenvalue analysis is performed to calculate natural frequency and mode shape for each mode in turn. The initial estimate provided is the solution from the previous rotor speed. Once one rotor speed sweep is completed, the compressive load is incrementally increased and the previously described sweep of rotor speed values is repeated. This procedure results in natural frequencies for each desired mode at every combination of rotor speed and compressive loading.

3 Model verification and validation

To verify that the model has been developed correctly and validate that it is capable of capturing the phenomena required, two complementary studies are performed. Firstly, an experimental study is used to demonstrate that the changes in the natural frequency with applied load are correctly captured by the model. Then, a high-fidelity Finite Element (FE) model is used to validate the results for a pretwisted, rotating beam that was not considered in the experiment.

3.1 Experiment

The focus of this research is to investigate the effects of the compressive load in isolation from the system used to apply it. However, this idealisation is not possible to achieve experimentally due to the inevitable presence of a system to apply the compressive load. For the experiment, a tendon, tensioned gravitationally using masses, is used to apply the compressive force. The use of a tendon as a loading application system will impact the results of the experiment and therefore the comparison with the model. It is acknowledged that the resulting validation will be limited due to the presence of the tendon.

Similar experiments on the dynamics of compressively loaded beams were performed in [18]. However, doubly symmetric cross-sections were used which exhibited no coupling between the different motion types. The experiment presented herein considers a singly symmetric cross-section to ensure bending-twist coupling is present.

3.1.1 Experimental setup description

The bench-top experiment can be seen in Fig. 4. The beam, described later in section 3.1.3, is rigidly clamped at the root and free at the tip. The tendon is attached to a plug-type insert secured at the tip of the beam and passes freely inside the beam towards the clamp at the root where its flexural motion is constrained. The tendon continues through the clamp, over a pulley and is attached to a hanging platform. The tension of the tendon, and hence the compressive load applied to the beam, is controlled by the amount of mass placed on the platform.

(a)

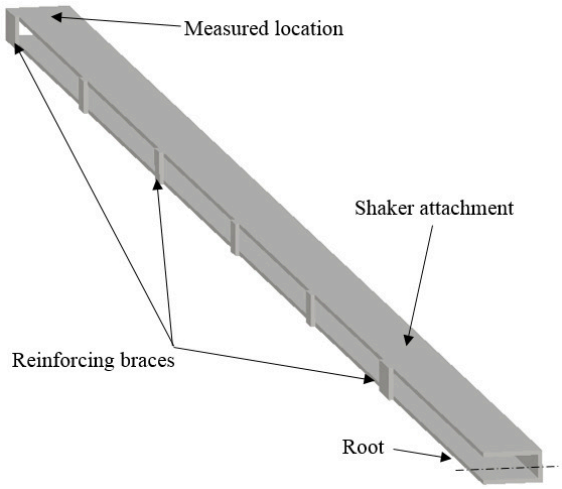

(b)

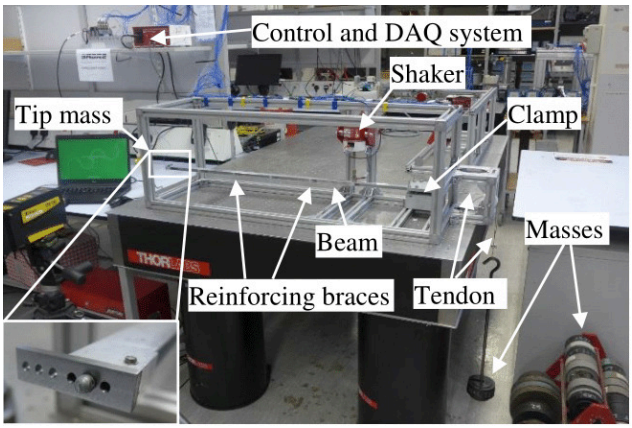

Fig. 4. Experimental set-up. (a) Schematic of the test beam. (b) Full experimental configuration.

The beam is excited using an electromagnetic modal shaker to obtain frequency response functions. The shaker is preferred to a modal hammer because of the repeatability that is required due to a large number of measurements needed to validate the theoretical model for a wide range of compressive loading configurations. Filtered pseudo-random excitation, which linearises possible weak non-linearities, is used to excite the frequency range between 5 and 150 Hz. To uphold the linear assumptions of

the model, excitation magnitudes remain small to ensure the displacements of the beam and tendon were also small. This has the additional benefit of ensuring that no contact between the beam and the tendon, other than those prescribed at the root and tip, is observed. The response data was collected from the tip using two single-axis piezoelectric accelerometers placed perpendicularly to each other.

The input force and response data were used to estimate frequency response functions using the H_v-estimator [31] for each compressive loading configuration. The compressive load is increased from 1 to 44 kg in one kilogram increments. The natural frequencies were estimated using the Least-Square Complex Frequency estimator [32].

3.1.2 Mathematical model for experiment

The tip insert used to attach the tendon to the tip of the beam is not included in the original mathematical model described in section 2. Therefore, the inertial forces and torques generated by the motion of the tip insert are included in the model for the purposes of the experimental validation. The boundary conditions for the tip of the beam, originally defined in Eq. (8), become

$$\begin{aligned} Q &= Q_{tip} \\ M_y &= M_z = 0 \\ F_y &= -P_y + F_{y,tip} \\ F_z &= -P_z + F_{z,tip} \end{aligned} \tag{10}$$

where Q_{tip} is the inertial torque about the elastic axis due to the tip insert, $F_{y,tip}$ and $F_{z,tip}$ are the inertial forces in the y and z directions due to the inertia of the tip insert. The expressions for these terms are calculated about the centre of mass of the tip insert and subsequently translated to the elastic axis of the beam and are defined such that

$$\begin{aligned} Q_{tip} &= \omega^2 m_{tip}\left(e_{tip} w \cos\beta - e_{tip} v \sin\beta + {e_{tip}}^2 \phi + {k_{m,tip}}^2 \phi\right) \\ F_{y,tip} &= \omega^2 m_{tip}\left(v - e_{tip}\phi \sin\beta\right) \\ F_{z,tip} &= \omega^2 m_{tip}\left(w + e_{tip}\phi \cos\beta\right) \end{aligned} \tag{11}$$

where m_{tip} is the mass of the tip insert e_{tip} is the distance between the centre of gravity of the tip mass and the elastic axis of the beam, and $k_{m,tip}$ is the polar radius of gyration of the tip mass about its centre of gravity.

3.1.3 Beam description

A thin-walled beam with a channel cross-section and reinforcing braces is used in the experiment. To ensure an observable change in frequency within the allowable loading range, the sensitivity to the compressive loading is accentuated by using a thin-walled cross-section to create a low-stiffness beam. To induce the bending-torsion coupling that is observed in modern rotorcraft blades, a channel section was chosen to provide a chordwise asymmetry to the profile. To reduce the sectional warping effects introduced by the thin-walled profile, the beam is reinforced with five 10mm wide braces equally spaced along the length of the beam (see Fig. 4). However, the braces will remove the constant, prismatic nature of the beam.

The experimental beam has 6 vibration modes between 5 and 150 Hz. Two are in-plane bending modes (marked as I1 and I2) and four are coupled out-of-plane bending-torsion (marked as O-T1 to O-T4). Due to the high levels of coupling between the out-of-plane and torsional motions, it was not possible to distinguish between the out-of-plane and torsionally dominated modes. The nominal properties of the non-braced sections of the beam seen in Fig. 4 are summarised in Table 1. Other parameters can be computed from the above parameters in a standard manner outlined in [22, 33].

Table 1

Beam properties for experimental beam

Property	Value	Property	Value
E [GPa]	70	I_1 [m^4]	2.32×10^{-9}
G [GPa]	26.3	I_2 [m^4]	5.00×10^{-9}
A [m^2]	9.18×10^{-5}	e [m]	0.0195
R [m]	1	$k_{m,tip}$ [m]	0.0125
m [kg m^{-1}]	0.2478	e_{tip} [m]	0.0160
J [m^4]	7.77×10^{-11}	m_{tip} [kg]	0.0269

3.1.4 Updating of beam parameters for baseline unloaded case

Before including the compressive loading in the experiment, the model of the beam without the tendon is validated. The purpose of this step is to evaluate and improve the underlying model of the beam, prior to any compressive force or effects of the tendon's dynamics.

The errors in the natural frequency values between the model and experiment are presented in Fig. 5 for three cases. Firstly, using the original parameters and with no tip mass. Secondly, using the updated parameters and with no tip mass. Thirdly, using the previously updated parameters with tip mass. These frequency errors form the basis for the metric used to update the parameters and improve the underlying model of the beam.

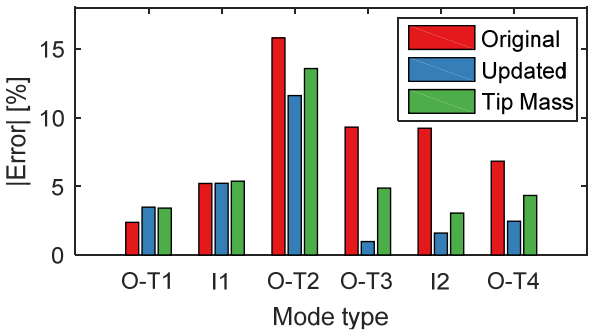

Fig. 5. Comparison of the absolute errors between the computed and experimentally measured frequencies.

It can be seen that the error for the model with the originally calculated parameters and no tip mass included is greater than 5% for almost all modes. These errors can be attributed to a combination of beam geometry tolerances, material parameters uncertainty, warping effects, the non-prismatic nature of the beam and the imperfect enforcement of the boundary conditions in the experiment. Therefore, a selection of the model's parameters are updated to reduce these errors. The parameters that are updated are limited to the geometric parameters which influence the beam's stiffness properties (I_1, I_2 and J) and the distance between the mass and elastic axis (e) as these are difficult to measure directly. For the updating procedure itself, an interior-point optimisation [34] is used to reduce the mean of the square of the frequency errors. This updating procedure reduces the errors of all but one mode to within 5% (the blue bars in Fig. 5). The updated beam properties are summarised in Table 2.

Table 2

Updated properties for experimental beam and change from their original value

Property	Value	Change, %
I_1 [m^4]	2.34 x 10^{-9}	+1.07
I_2 [m^4]	4.06 x 10^{-9}	-18.85
J [m^4]	9.00 x 10^{-11}	+15.83
e [m]	0.0200	+2.77

After updating, the errors are considered when the tip insert is included (the green bars in Fig. 5). It can be seen that the increases in errors due to the tip mass are moderate which indicates the inertial effects of the tip insert are sufficiently captured in the boundary conditions.

Despite the updating of the parameters, significant errors remain present across all modes. The magnitude of these errors and their presence across all modes indicates that the model's ability to represent the experimental beam is limited. However, the purpose of the experiment is to evaluate the model's ability to capture the changes in frequency achieved using compressive loading and not to study the impact of violating beam assumptions of the underlying beam model. Subsequent analysis shall consider only the change in frequency with compressive load, not the absolute errors between the experimental and modelled frequency values.

3.1.5 Validation of the effects of compressive loading on frequency

Once the baseline beam model is updated, the effect of compressive load is considered. The tendon loading is increased from 1 to 44 kg and the change in the natural frequency of the first six beam modes is observed. The change in these frequencies observed experimentally and calculated by the model relative to their respective unloaded case are shown in Fig. 6.

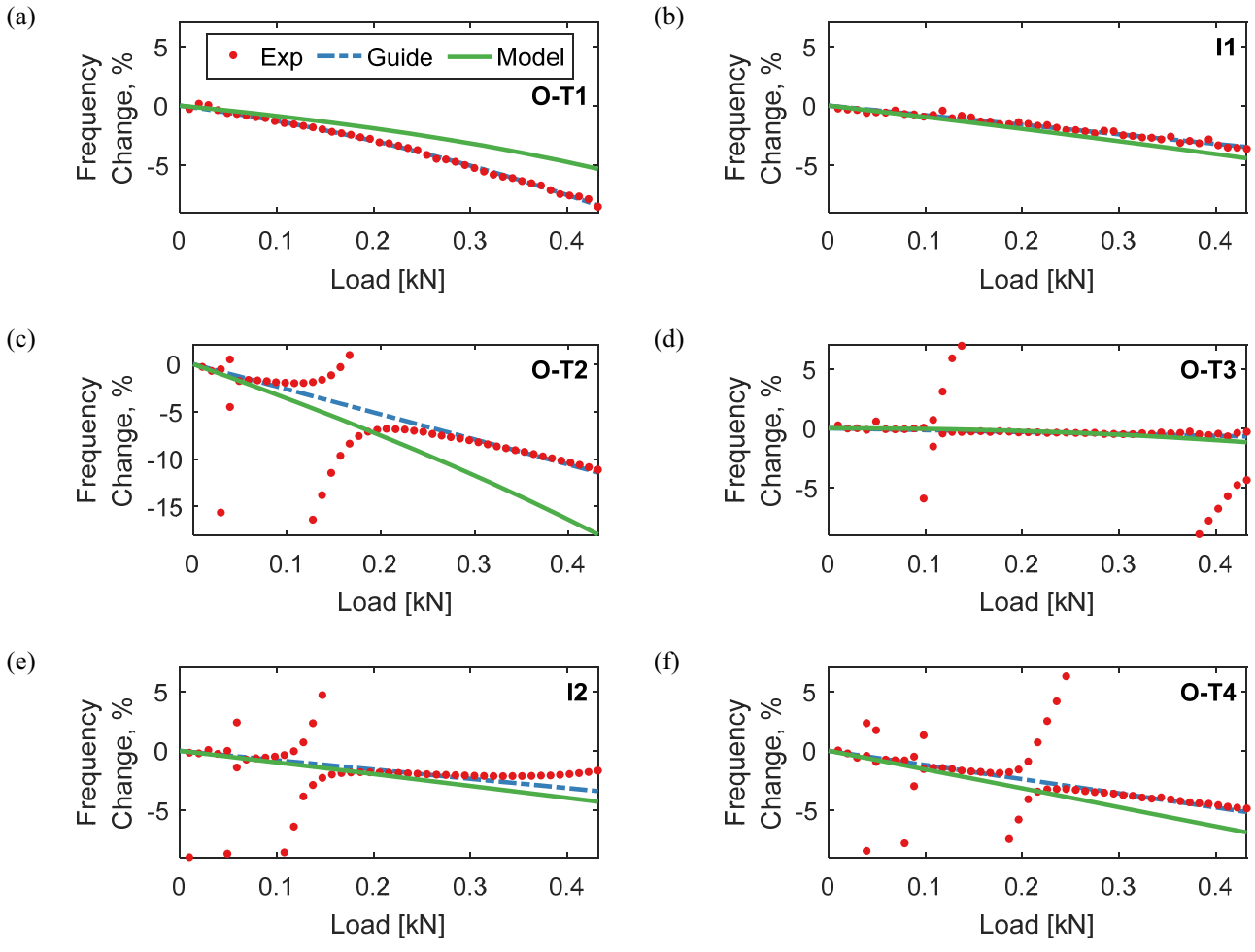

Fig. 6. Change in natural frequency with compressive load. The experimental data points (red), the guiding lines (blue) and the beam model results (green) are shown. (a) O-T1. (b) I1. (c) O-T2. (d) O-T3. (e) I2. (f) O-T4.

It can be seen in Fig. 6 (a) and (b) that there is no interaction with the dynamics of the tendon. However, Fig. 6 (c) to (e) shows there are multiple regions where the dynamics of the tendon interact with the dynamics of the beam due to a phenomenon known as veering [7, 20, 35, 36]. As previously stated, the purpose of this research is to investigate the effects of the compressive load in isolation from the method for applying the load. The load application method and the associated effects that it incurs are not studied here. Subsequently, the dynamics of the tendon are not considered in this experiment. A set of guiding lines are created using a polynomial least-squares fit of the experimental data points away from the regions affected by veering. These lines visualise the effects of the tendon's load and omit the coupled beam-tendon dynamics in the veering regions. The guiding line for the first mode (O-T1), shown in Fig. 6 (a), is quadratic but for the other modes is linear as the veering obscures the change in gradient of the experimental data points.

It can be seen that the trends of the guiding lines are consistent with the predictions of the model for the majority of the modes in terms of direction, magnitude and curvature. The discrepancies in the trends can be attributed to the tendon's dynamics and errors in the underlying beam model. The mode with the largest discrepancy (O-T2) is also the mode with the largest underlying beam model error in section 3.1.4. This indicates that the source of the error in the underlying beam model also affects the ability to model the effect of the compressive load.

As it was not possible to completely supress all the effects of the tendon from the experimental results, an imperfect match was inevitable. However, the similarity in the predicted and measured trends and their gradients demonstrates that the model is capable of correctly capturing the change in natural frequency due to compressive loading and that the methodology of modelling the compressive load as a point force is suitable for use in future studies. It is, however, appreciated that the method of applying compressive load influences the beam's dynamics significantly. It is accepted that the lack of load application system is a limitation of the model but also invites future research in to what method of compressive load application should be used [37].

3.2 Finite element model

An FE model is used to complement the experimental validation of the model by focusing on the capability of the model to represent a fully coupled rotating beam with pretwist. Additionally, this study uses a beam with a constant and closed cross-section, thereby providing conditions under which the Euler-Bernoulli assumptions are upheld.

3.2.1 Model description

The beam used for this analysis has a hollow rectangular cross-section with one axis of symmetry along the major neutral axis, as seen in Fig. 7. The asymmetry along the minor neutral axis creates an offset between the mass axis and elastic axis. The

dimensions of the beam are chosen such that the cross-section is closed but exhibits similar stiffnesses, mass and offset between the mass and elastic axes to a realistic rotor blade. This beam was modelled in Abaqus [38] using approximately 470,000 brick elements with a fully fixed root. For the analysis using the beam model the cross-section properties were calculated using *SaaS ShapeDesigner* [39], an FE solver for generalised cross-sections, as summarised in Table 3.

(a)

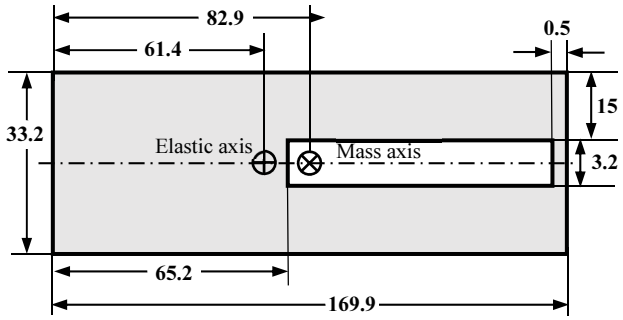

(b)

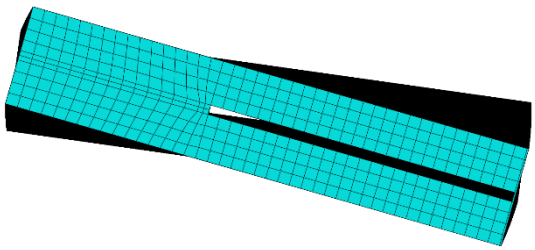

Fig. 7. Beam section used in FE analysis. (a) Cross-section dimensions – all values in mm. (b) Beam meshed in Abaqus

Table 3

Beam properties for FE analysis

Property	Value	Property	Value
E [GPa]	69	Ω [rads^{-1}]	50
G [GPa]	26.5	R [m]	5.5
ρ [kgm^{-3}]	2700	R_0 [m]	0.5
$\beta(R_0)$ [^{o}]	16	e_o [m]	0.0200
$\beta(R)$ [^{o}]	8		

The compressive load is modelled based on the same approach introduced in section 2.1.2. The force P_x is applied as a constant force at the elastic axis of the tip (shown in Fig. 7) orientated towards the axis of rotation. The in-plane and out-of-plane forces due to the compressive load, P_y and P_z (see Eq (3)), can be modelled as linear springs with the stiffness defined as $P/(R - R_0)$ as has been noted previously in [27]. Here, these forces are applied via two grounded unidirectional springs (one for P_y and one for P_z) attached at the elastic axis at the tip of the beam.

3.2.2 Validation of compressively loaded rotating pretwisted beam

The beam model and the FE model are used to calculate the natural frequencies of the first torsion (T1), first four out-of-plane modes (O1-O4) and first two in-plane modes (I1-I2). These values are calculated in the range of rotor speeds between 60%-100% of the nominal value stated in Table 3.

The critical load that leads to the loss of structural stability can be defined as the compressive load at which the lowest natural frequency equals zero [27, 40, 41]. In this work, this load is calculated at the lowest rotor speed considered (60% of nominal) to ensure a conservative limit. For this study, this critical load is calculated to be 55.12 kN. The maximum compressive load considered for this validation study is chosen to be 75% of this load, 41.34 kN to further ensure this instability is not encountered.

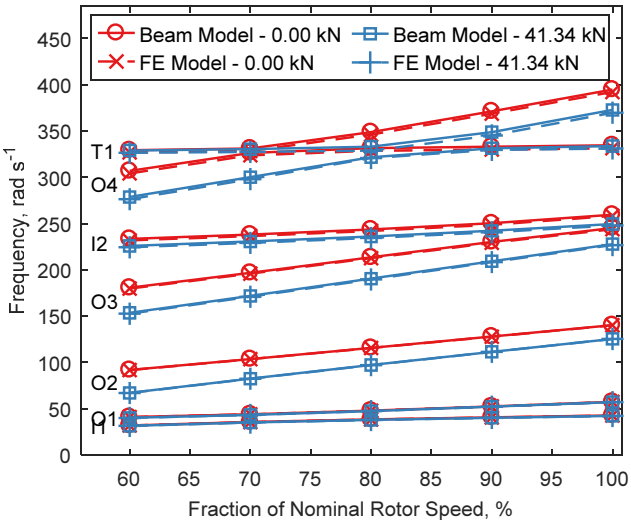

Fig. 8. Comparison of the natural frequencies for the rotating beam calculated using the beam model and an FE model.

The frequency loci shown in Fig. 8 feature very good correlation between the beam model and the FE model. The beam model slightly overpredicts the frequencies of the transversal bending motions and the magnitude of this error is larger in the higher order modes. This is expected as the equations of motion used are based on Euler-Bernoulli bending theory which overestimates the natural frequencies of higher order modes due to the omission of transverse shear deformation [42]. The discrepancies are consistent between the loaded and unloaded cases and all errors are less than 1.3%.

The combination of the experimental and FE analyses validates the ability of the model to predict the natural frequencies of a pretwisted rotating beam with an applied compressive load.

4 Resonance avoidance in variable speed rotors

This section uses the previously described and validated model in the context of a rotor blade. Initially, the resonance problems in variable speed rotors are exemplified. Then the ability of a compressive load and optimal tuning to avoid these resonances is assessed.

The test case considered is a bearingless blade with properties and operating conditions representing the MBB Bo 105 helicopter [43] as summarised in Table 4. The model described in section 2 is used to calculate the frequencies of the first torsion (T1), first four out-of-plane modes (O1-O4) and first two in-plane modes (I1-I2), across the chosen range of loads and rotor speeds. The assessed range of rotor speeds is 60%-100% of nominal value. The upper limit of the compressive load considered is calculated to be 15.86 kN as described in section 3.2.2.

Table 4

Blade properties and operating conditions for the MBB Bo 105

Property	Value	Property	Value
E [GPa]	69	I_1 [m^4]	9.92 x10^{-8}
G [GPa]	26.5	I_2 [m^4]	2.47 x10^{-6}
ρ [kgm^{-3}]	2700	J [m^4]	1.65 x10^{-7}
R_0 [m]	0.38	e [m]	-0.0195
R [m]	4.91	e_o [m]	0.0189
$\beta(R_0)$ [°]	15	A [m^2]	2.80 x10^{-3}
β(R) [°]	7	Ω [$rads^{-1}$]	44.51

4.1 Resonance in a variable speed rotor without compressive loading

Rotor blade modes without compressive loading are calculated to highlight the potential resonant interactions encountered when varying rotor speed. The natural frequencies and harmonics of the rotor speed are presented in Fig. 9 (a). From this diagram, it can be seen that there are multiple rotor speeds where the natural frequencies cross the rotor speed harmonics indicating potential blade resonances.

To quantify the proximity of a mode to resonance the metric referred to as the *minimum modal separation* (MMS) is used. At each rotor speed, the difference between each mode and its closest rotor harmonic is calculated as a fraction of the rotor speed, as seen in Fig. 9 (b). The *minimum modal separation* is the minimum of these difference across all modes. This can be defined mathematically according to Eq. (12), and is shown in Fig. 9 (b). MMS is used as the metric to avoid resonance; this is a traditional approach to the dynamic design of rotorcraft blades [44] and is therefore also adopted herein.

$$MMS(\Omega) = \frac{\min\left(\left|\omega_{0,i}(\Omega) - n\Omega\right|\right)}{\Omega} \qquad (12)$$

$$for\ all\ i\ and\ where\ n\ is\ a\ real\ positive\ integer$$

(a)

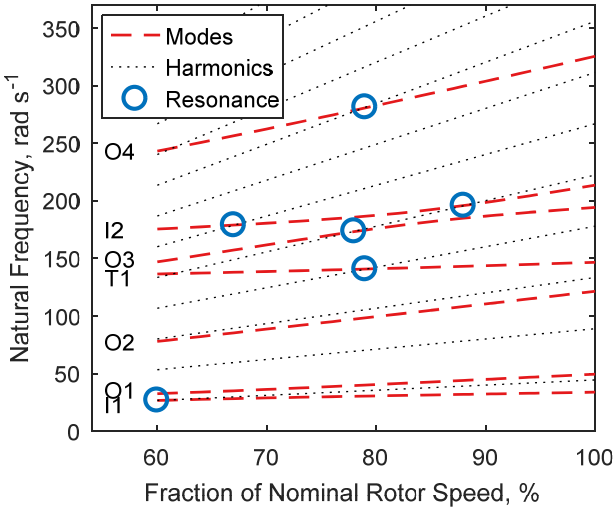

(b)

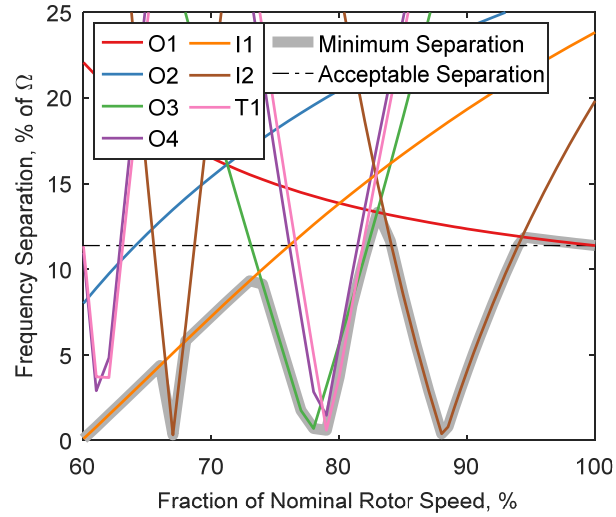

Fig. 9. Resonant regions of the variable speed rotor without compressive loading (a) Campbell diagram. (b) Separation of each mode from its nearest rotor harmonic.

It can be seen in Fig. 9 (b) that at the nominal rotor speed, the minimum separation is dictated by the first out-of-plane mode. The MMS at this rotor speed is 11.38% which shall be used as the reference for an acceptable level of separation throughout this case-study. At 94.5% of the nominal rotor speed, the second in-plane mode dictates the MMS and it begins to decrease as the rotor slows, dropping below the acceptable MMS level at 94%. It can be seen that there are multiple regions where the MMS is below the acceptable level and that these regions are dictated by many different modes. Therefore, the ability of compressive loading to alter many modes will be vital to achieving an acceptable MMS over the range of rotor speeds desired.

4.2 Resonance avoidance using compressive load

The concept of using compressive loading to alter the natural frequencies as a means of avoiding resonance shall now be investigated. For each combination of rotor speed and compressive loading, the MMS is calculated as follows.

$$MMS(\Omega, P) = \frac{\min\left(\left|\omega_{0,i}(\Omega, P) - n\Omega\right|\right)}{\Omega} \quad (13)$$

$$for\ all\ i\ and\ where\ n\ is\ a\ real\ positive\ integer$$

Subsequently, the compressive load which yields the greatest MMS value is identified for each rotor speed and used as the optimum loading profile presented in Fig. 10. The natural and excitation frequencies over the investigated range of rotor speeds and loadings are presented in Fig. 11.

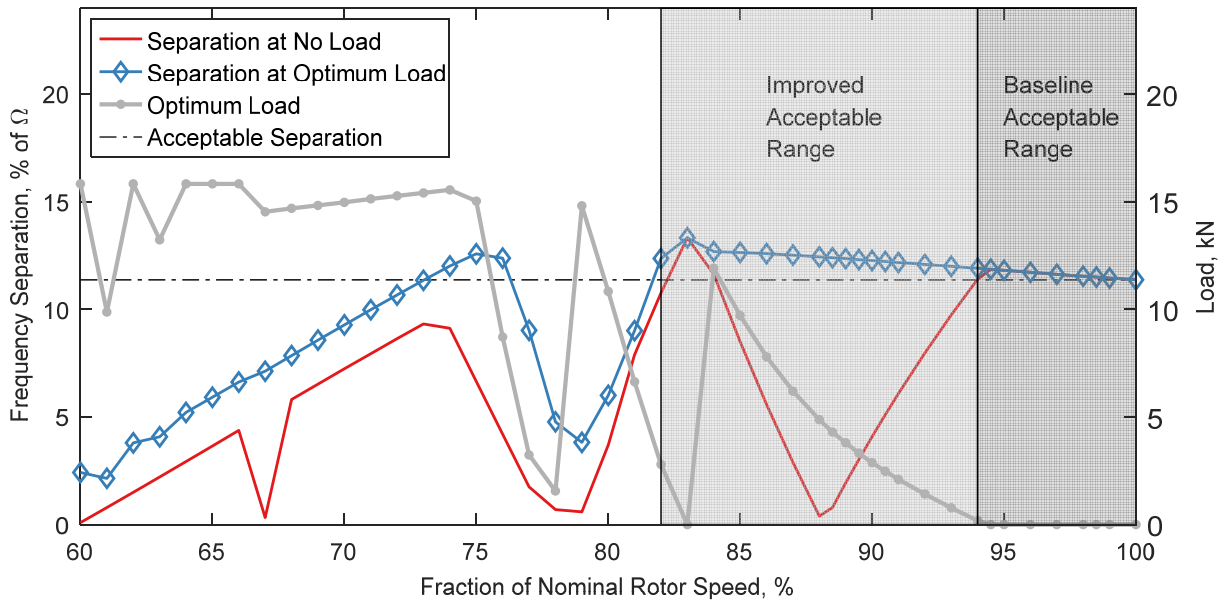

Fig. 10. Nominal and optimal Minimum Modal Separation with applied compressive loading.

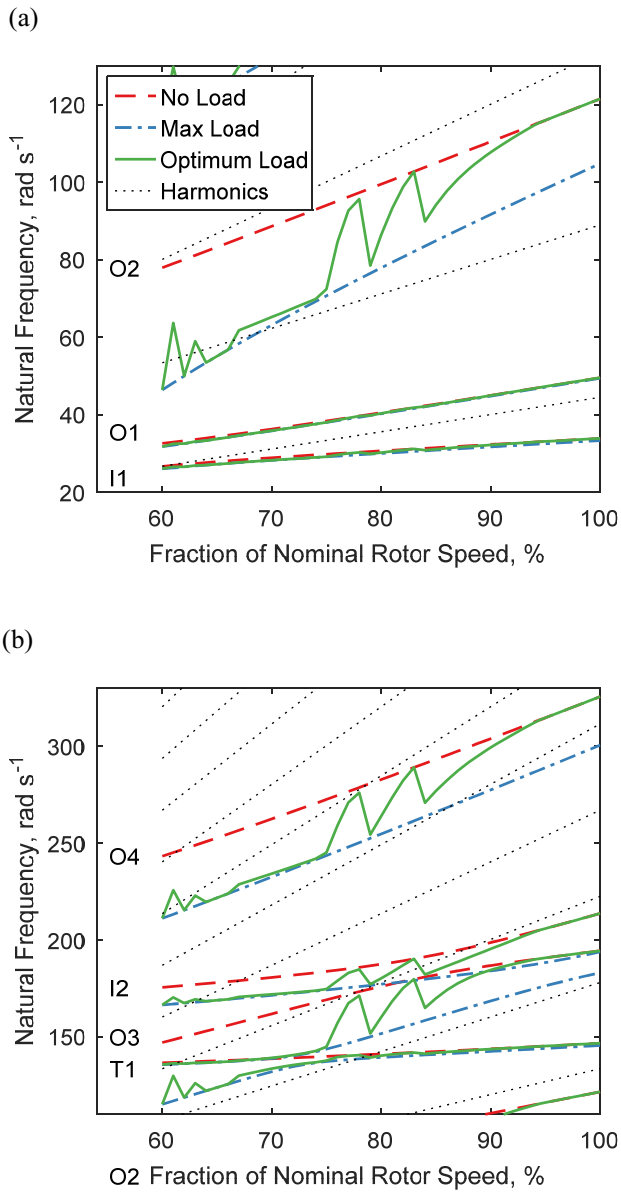

Fig. 11. Campbell diagram with optimum changes in the blade natural frequencies.

Starting from 100% of the nominal rotor speed, Fig. 10 shows the optimum loading is 0 kN until 94.5%, resulting in an optimum separation identical to the unloaded case. This occurs because the first out-of-plane mode governs separation for this region and any compressive loading would reduce this frequency separation. The next region, from 94.5% to 84%, exhibits a gradual increase in optimal compressive load up to 11.92 kN, which is 56% of the critical load. This compressive load reduces the second in-plane mode and resulting in an acceptable MMS level. At 84% of the nominal rotor speed, the unloaded second in-plane mode has completely crossed the excitation frequency, as seen in Fig. 11, and the maximum separation is once again obtained with no compressive loading. The separation for the next region, from 84% to 74%, is dictated by the third out-of-plane and first torsional mode. The third out-of-plane mode is sensitive to compressive loading but the torsional mode is not, resulting in minimal

improvements in separation. From 74% to 68% and 66% to 60% the separation is dictated by the first in-plane mode which is relatively insensitive to loading. This insensitivity results in a modest improvement to MMS. Conversely, the resonance of the second in-plane mode at 67% is very sensitive and can therefore be almost completely avoided.

It has been demonstrated that the compressive load can improve separation across the range of rotor speeds, thus facilitating a significant improvement in the allowable reduction of rotor speed. For the baseline case with no loading, a 6% reduction from the nominal rotor speed is possible, but for the optimally loaded case, an 18.2% reduction is possible. Additionally, this study has highlighted the importance of the differing sensitivities of each mode. Modes such as the first in-plane and first torsion demonstrated minimal sensitivity to the compressive loading and therefore avoiding resonances with these modes was not possible.

5 Discussion

The model used in this study has been validated using a combination of an experiment and FE analysis. The experiment was conducted using a beam with a thin-walled open cross-section and short bracing segments to maximise sensitivity to loading and introduce the coupling between the torsional and out-of-plane bending motions whilst minimising cross-sectional warping effects. The beam was loaded using a tendon to apply the compressive load. The comparison of the measured and predicted frequencies provided two main conclusions. Firstly, it validated the model's ability to capture the main effects of the compressive load and the proposed methodology used to model the compressive load as a point force. The predicted and observed changes in the natural frequencies caused by the compressive load agreed. The discrepancies can be attributed to the dynamics of the tendon in the experiment, the non-prismatic nature of the beam and the violation of the Euler-Bernoulli assumptions due to thin-walled open cross-section used in the experiment. Secondly, the lack of pretwist and rotation as well as the violation of the Euler-Bernoulli assumptions and the non-constant cross-section prohibited the experiment from providing a comprehensive validation of the beam model. An FE model was used to represent a pretwisted rotating beam with a closed asymmetric cross-section and a compressive load applied using a combination of a constant point forces and transversally oriented spring elements applied at the tip of the beam. The comparison of the Campbell diagrams produced for an unloaded and highly loaded case show very good agreement, with all errors less than 1.3%. As well as validating the underlying beam model, this comparison also provides good verification of the implementation of the compressive load. It can be seen in Fig. 6 that the predicted changes in natural frequency exceed those observed experimentally; something which is not present in the FE validation. Whilst this suggests that the model developed is non-conservative, it could be considered as a theoretical capability for which the load application system should be designed to meet this capability as closely as possible.

A case study was used to investigate the potential of compressive load to alleviate the dynamics problems associated with variable speed rotors. The natural frequencies of an MBB Bo105 rotor blade were calculated for compressive loads up to 75% of the critical value and up to a 40% reduction in the rotor speed to investigate the likely operational range of the variable speed rotor

concept [9, 10]. At each rotor speed the minimum modal separation was calculated to indicate the proximity of resonance. In the course of this study an optimal loading profile was created for the selected range of rotor speeds. It was shown that loading profile maximises the aforementioned MMS. This optimum loading profile significantly improves the frequency separation over the desired range of rotor speeds and would therefore facilitate a significant increase in the range of operational rotor speeds.

A number of assumptions were made within the model which lead to limitations in its use. The use of an Euler-Bernoulli formulation reduces the validity when deflections are large or there is cross-sectional warping. The validation of the model was performed for compressive loads of up to 75% of the critical value. There are multiple factors such as structural damping, coupling of composite beams and external forces, such as aerodynamics, which were not considered in this study and may influence the performance of the concept.

Subsequent investigations must be completed to understand the impact of compressive loading on a rotor blades' dynamic behaviour with aerodynamic forcing from realistic operating conditions such as hover and forward flight. The case study highlights that the magnitude of separation change varies between modes. Therefore, future investigations should consider vibratory loads, not frequency separation as the determining factor. Finally, the actuation method should be considered to evaluate its requirements and their implications on rotor performance, such as mass and power penalties as well as the impact of their own dynamics on the blade and the compressive loading effect.

6 Conclusion

This paper presents a model of a pretwisted rotating beam with fully coupled in-plane, out-of-plane and torsional motions with an applied compressive load. The compressive load is applied at the tip of the beam, orientated towards its root and modelled as a decomposition into forces along the undeformed x, y and z axes. The system is modelled using a set of coupled ordinary differential equations formulated in to a boundary value problem and solved using a collocation method to obtain the modal properties. Using a combination of experimental and FE results, the model of the beam and the applied force are validated and the modelling limitations are identified and discussed. A case study is performed using the model to investigate the capability of compressive loading to be used as a resonance avoidance technique for variable speed rotors. The study shows that significant alterations to the blade's natural frequencies can be achieved with compressive loads. This ability to alter the blade's frequencies allows improved separation between the natural and excitation frequencies when compared to the baseline unloaded case. The improved separation over the range of rotor speeds investigated implies that compressive loading could be utilised as a resonance avoidance method for variable speed rotors.

7 Conflict of interest statement

The authors wish to confirm that there are no known conflicts of interest associated with this publication.

Acknowledgements

R. Dibble would like to thank The UK Vertical Lift Network and ESPRC for the guidance and funding provided. V. Ondra and B. Titurus would like to acknowledge the financial support of the European Community's Horizon 2020 Program provided through the project "Shape Adaptive Blades for Rotorcraft Efficiency (SABRE)", Grant Agreement 723491.

References

[1] A. E. Karem, "Optimum Speed Rotor". United States Patent 6,007,298, 28 December 1999.

[2] D. Han, V. Pastrikakis and G. N. Barakos, "Helicopter performance improvement by variable rotor speed and variable blade twist," *Aerospace Science and Technology,* vol. 54, pp. 164-173, 2016.

[3] R. Ramanujam and A. Abhishek, "Performance Optimization of Variable-Speed and Variable-Geometry Rotor Concept," *Journal of Aircraft,* vol. 54, no. 2, pp. 476-489, 2017.

[4] G. A. Misté and E. Benini, "Variable-Speed Rotor Helicopters: Performance Comparison Between Continuously Variable and Fixed-Ratio Transmissions," *Journal of Aircraft,* vol. 53, no. 5, pp. 1189-1200, 2016.

[5] D. Han, C. Dong and G. N. Barakos, "Performance improvement of variable speed rotors by Gurney flaps," *Aerospace Science and Technology,* vol. 81, pp. 118-127, 2018.

[6] M. Allongue, H. Marze and F. Potdevin, "Quiet Helicopter 'from research to reality'," in *55th Annual AHS Forum Proceedings*, Montreal, 1999.

[7] J. D. Bois, N. Lieven and S.Adhikari, "A tensioned cable as an adaptive tuned vibration absorber for response supression in rotorcraft," in *ISMA International Conference on Noise and Vibration Engineering*, Leuven, 2012.

[8] Flightglobal, "FARNBOROUGH: Cutaway & technical description: Defying convention - Boeing A160 Hummingbird," 12 07 2010. [Online]. Available: https://www.flightglobal.com/news/articles/farnborough-cutaway-technical-description-defyin-344075/. [Accessed 22 06 2016].

[9] Fédération Aéronautique Internationale, *Record ID #15059,* 2008.

[10] D. Han, J. Wang, E. C. Smith and G. A. Lesieutre, "Transient Loads Control of a Variable Speed Rotor During Lagwise Resonance Crossing," *AIAA Journal,* vol. 51, no. 1, pp. 20-29, 2013.

[11] NAVAIR, “V-22 Osprey 2010 Guidebook,” Tech. Rep. PMA-275, 2010.

[12] D. Han and E. Smith, “Lagwise dynamic analysis of a variable speed rotor,” *Aerospace Science and Technology,* vol. 29, no. 1, pp. 277-286, 2013.

[13] J. Pearson, R. Goodall and I. Lyndon, “Active Control of Helicopter Vibration,” *Computing Control Engineering Journal,* vol. 5, no. 6, pp. 277-284, 1994.

[14] P. Konstanzer, B. Enenkl, P. Aubourg and P. Cranga, “Recent advances in eurocopter's passive and active vibration control,” in *American Helicopter Society 64th Annual Forum*, Alexandria, 2008.

[15] R. H. Markiewicz, “A study of the aeroolastic behaviour of helicopter rotor blades featuring swept tips,” Cranfield Institute of Technology, 1990.

[16] D. E. Kakaley, M. R. Jolly and G. D. Buckner, “An offset hub active vibration control system for mitigating helicopter vibrations during power loss: Simulation and experimental demonstration,” *Aerospace Science and Technology,* vol. 77, pp. 610-625, 2018.

[17] J. D. Bois, N. Lieven and S. Adhikari, “Adaptive Passive Control of Dynamic Response through Structural Loading,” in *48th AIAA/ASME/ASCE/AHS/ASC Structures, Structural Dynamics and Materials Conference*, Honolulu, 2007.

[18] R. P. Dibble and B. Titurus, “Helicopter rotor blade modal tuning using internal preloads,” in *Proceedings of the ISMA International Conference on Noise and Vibration Engineering*, Leuven, 2016.

[19] R. P. Dibble, B. Woods and B. Titurus, “Static Aeroelastic Response of a Rotor Blade Under Internal Axial Loading,” in *43rd European Rotorcraft Forum*, Milan, 2017.

[20] V. Ondra, R. Dibble and B. Titurus, “Towards an application of an active tendon in rotorcraft:,” in *Proceedings of the ISMA 2018 International Conference on Noise and Vibration Engineering*, Leuven, 2018.

[21] R. W. Prouty, Helicopter Performance, Stability and Control, 1986.

[22] J. C. Houbolt and G. W. Brooks, “Differential equations of motion for combined flapwise bending, chordwise bending, and torsion of twisted nonuniform rotor blades,” National Advisory Committee for Aeronautics Technical Note 3905, 1957.

[23] S. Moffatt and N. Griffiths, "Structural optimisation and aero-elastic tailoring of the berp iv demonstrator blade," in *American Helicopter Society 65th Annual Forum*, Grapevine, TX, 2009.

[24] B. van der Wall and J. Yin, "DLR's S4 rotor code validation with HART II data: the baseline case," in *International Forum on Rotorcraft Multidisciplinary Technology*, Seoul, Korea, 2007.

[25] L. Meirovitch, Analytical Methods in Vibrations, Macmillan, 1967.

[26] M. Rafiee, F. Nitzsche and M. Labrosse, "Dynamics, vibration and control of rotating composite beams and blades: A critical review," *Thin-Walled Structures,* vol. 119, pp. 795-819, 2017.

[27] S. Nudehi, R. Mukherjee and S. W. Shaw, "Active Vibration Control of a Flexible Beam Using a Buckling-Type End Force," *Journal of Dynamic Systems, Measurement, and Control,* vol. 128, no. 2, pp. 278-286, 2006.

[28] L. F. Shampine, J. Kierzenka and M. Reichelt, *Solving Boundary Value Problems for Ordinary Differential Equations in MATLAB with bvp4c,* Natick, MA: The Mathworks, Inc, 2000.

[29] S. S. Rao, Vibration of Continuous Systems, John Wiley & Sons, 2007.

[30] V. R. Murthy, "Dynamic characteristics of rotor blades," *Journal of Sound and Vibration,* vol. 49, no. 4, pp. 483-500, 1976.

[31] J. S. Bendat and A. G. Piersol, Random Data: Analysis and Measurement Procedures, 2nd ed., New York: John Wiley & Sons, 1986.

[32] B. Peeters, H. Van der Auweraer, P. Guillaume and J. Leuridan, "The PolyMAX Frequency-Domain Method: A New Standard for Modal Parameter Estimation?," *Shock and Vibration,* vol. 11, no. 3-4, pp. 395-409, 2004.

[33] D. H. Hodges and E. H. Dowell, "Nonlinear equations of motion for the elastic bending and torsion of twisted nonuniform rotor blades," NASA Technical Note D-7818, 1974.

[34] R. H. Byrd, J. C. Gilbert and J. Nocedal, "A Trust Region Method Based on Interior Point Techniques for Nonlinear Programming," *Mathematical Programming,* vol. 89, no. 1, pp. 149-185, 2000.

[35] J. L. d. Bois, S. Adhikari and N. A. Lieven, "Eigenvalue curve veering in stressed structures: An experimental study," *Journal of Sound and Vibration,* vol. 322, pp. 1117-1124, 2009.

[36] N. C. Perkins and C. D. Mote, “Comments on curve veering in eigenvalue problems,” *Journal of Sound and Vibration,* vol. 106, no. 3, pp. 451-463, 1986.

[37] F. Nicassio, G. Scarselli, F. Pinto, F. Ciampa, O. Iervolino and M. Meo, “Low energy actuation technique of bistable composites for aircraft morphing,” *Aerospace Science and Technology,* 2018.

[38] Simulia, “Abaqus Analysis User Guide,” 2016.

[39] SaaS, *User Guide & Techniques,* 2010.

[40] H. Lurie, “Lateral vibrations as related to structural stability,” *Journal of Applied Mechanics,* vol. 19, pp. 195-204, 1952.

[41] L. N. Virgin, Vibration of Axially-Loaded Structures, Cambridge: Cambridge University Press, 2007.

[42] M. Rafiee, F. Nitzsche and M. Labrosse, “Dynamics, vibration and control of rotating composite beams and blades: A critical review,” *Thin-Walled Structures,* vol. 119, pp. 795-819, 2017.

[43] J. A. Staley, “Validation of Rotorcraft Flight Simulation Program through Correlation with Flight Data for Soft-in-Plane Hingeless Rotors,” AMRDL, 1976.

[44] S. Moffatt and N. Griffiths, “Structural Optimisation and Aeroelastic Tailoring of the BERP IV Demonstrator Blade,” in *American Helicopter Society 65th Annual Forum*, Grapevine, Texas, 2009.